

The role of synoptic and intraseasonal anomalies on the life cycle of rainfall extremes over South America: non-summer conditions

Fernando E. Hirata¹  · Alice M. Grimm¹

Received: 4 May 2016 / Accepted: 4 September 2016 / Published online: 13 September 2016
© Springer-Verlag Berlin Heidelberg 2016

Abstract Previous study showed that the interaction of synoptic disturbances with intraseasonal anomalies is important for heavy rainfall in the South Atlantic Convergence Zone and the La Plata basin during the austral summer. Here, we conduct similar analysis to study the evolution of rainfall extremes during austral spring (SON), fall (MAM) and winter (JJA). A relatively homogeneous region over southeastern South America, whose limits change little from season to season, is heavily affected by extreme precipitation events, as indicated by the value of the 95th percentile of daily rainfall, higher during the spring season ($16.94 \text{ mm day}^{-1}$) and lower in winter ($13.79 \text{ mm day}^{-1}$). From 1979 to 2013, extreme rainfall events are more frequent in spring (131 events) and less frequent in fall (112 events). Similar to summertime extreme events, synoptic-scale waves continue to be the main drivers of extreme precipitation over the region. The interaction between these waves and intraseasonal anomalies during the development of rainfall extremes over southeastern South America is observed especially during neutral ENSO and La Niña conditions. Warm ENSO phases tend to favor more frequent extremes in all three seasons and extreme events during El Niños are associated with synoptic waves, with no significant interaction with intraseasonal anomalies.

1 Introduction

Previous studies have demonstrated the connection between rainfall and synoptic disturbances (e.g., Liebmann et al. 1999) and the importance of intraseasonal anomalies for wet summer conditions in the South Atlantic Convergence Zone (SACZ) (Nogués-Paegle et al. 2000; Carvalho et al. 2004; Liebmann et al. 2004; Cunningham and Cavalcanti 2006). A previous article (Hirata and Grimm 2015) detailed the interaction between synoptic and intraseasonal anomalies during the development of extreme precipitation events over South America in summer (DJF). Synoptic disturbances are the main drivers of summer precipitation extremes over three intensely inhabited regions of South America (the SACZ, the southeastern Brazilian coast, and the La Plata basin). On intraseasonal timescales, a dipole in convection, which modulates rainfall in the SACZ and the subtropical plains to the south (part of the La Plata basin) (Nogués-Paegle and Mo 1997), apparently influences the occurrence of heavy rainfall episodes as well (Liebmann et al. 2004; Jones et al. 2004). Hirata and Grimm (2015) demonstrated that summertime intraseasonal anomalies appear in upper-level geopotential height flanking the South American subtropical jet. When the anomalies indicate a deceleration of the jet (cyclonic anomalies to the north and anticyclonic ones to the south of the jet axis), negative zonal stretching deformation ($\partial U/\partial x < 0$) intensifies and synoptic wave energy tends to accumulate in the region (Webster and Chang 1988). The accumulation of wave energy favors enhanced convective activity in the SACZ and subsidence over the subtropical plains of the La Plata basin. On the other hand, acceleration of the jet, indicated by anticyclonic anomalies to the north and cyclonic ones to the south of the jet axis, reduces wave energy accumulation and consequent convective activity in the SACZ.

✉ Fernando E. Hirata
fernando.endo.hirata@gmail.com

¹ Department of Physics, Universidade Federal do Paraná, Curitiba, Brazil

Thus, subsidence over the La Plata basin weakens, favoring heavier rainfall over the subtropics.

During summer, the relative importance of synoptic and intraseasonal anomalies varies according to El Niño–Southern Oscillation (ENSO) phases (Hirata and Grimm 2015). When warm ENSO conditions prevail, intraseasonal anomalies favor extremes in the subtropical La Plata basin and the southeastern Brazilian coast. Intraseasonal anomalies in the life cycle of SACZ extremes during El Niños are less significant and heavy rainfall relies more on the synoptic disturbances.

During non-summer conditions, extreme rainfall impacts on densely populated areas are concentrated in a region encompassing southern Brazil, Uruguay and northeastern Argentina (southeastern South America), with small spatial variations from season to season. The summer climatological negative zonal stretching deformation in the SACZ region is weaker or absent once the local zonal deceleration of zonal winds is a consequence of the summer circulation (i.e. the formation of the upper-level Bolivian High). Therefore, accumulation of wave energy and the SACZ are rarely observed in other seasons. Synoptic disturbances continue to be the main drivers of rainfall extremes in the region. Increased baroclinicity and lee cyclogenesis over southern and southeastern South America result from the blocking of low-level circulation by the Andes Cordillera, associated with eastward moving disturbances (Gan and Rao 1994).

In austral winter, vortex stretching and vorticity advection drive midtropospheric troughing to the east of the mountains during the development of strong cold air outbreaks (Marengo et al. 1997). Two positive feedbacks identified by the authors during intense outbreaks help to intensify the equatorward incursion of cold air over South America. In the early stages of development, a troughing leads to northward cold advection along the eastern flanks of the Andes, which causes a temperature drop and consequently deepens the original trough. In the later stages, midtropospheric cold advection generates a near surface anticyclone, which is intensified by descending motion, low-level divergence and consequent anticyclonic growth. Synoptic cold air outbreaks in South America are characterized by a long wave pattern consisting of a cyclonic perturbation over the subtropics and an anticyclone over the southern Pacific (Vera and Vighiarolo 2000). This subtropical cyclonic perturbation is associated with the northward displacement of the South America subtropical jet, facilitating the penetration of frontal systems. Vera and Vighiarolo (2000) propose that strong synoptic cold surges to the east of the Andes result from the interaction between a subpolar cyclonic perturbation moving equatorward with eastward upper-level cyclonic perturbations at subtropical latitudes. Upper-level vorticity advection within midlatitude waves and the transverse direct circulation driven by the South

American subtropical jet entrance are instrumental for the growth of the surface cyclones and anticyclones moving through the region (Garreaud 2000). Alvarez et al. (2015) showed that the Madden–Julian Oscillation (MJO) impacts precipitation and temperature in southeastern South America during non-summer conditions.

Here, it is demonstrated that the interaction between synoptic disturbances and intraseasonal anomalies is important to drive heavy rainfall over southeastern South America during neutral and La Niña phases in non-summer conditions. During El Niños, intraseasonal anomalies associated with extreme events as defined here are less significant. Whenever intraseasonal anomalies are significant, the linkage between heavy rainfall and large scale tropical intraseasonal convection (such as the MJO) depends on the season. Moreover, intraseasonal anomalies seem to be part of a stationary long wave train linking the Pacific to South America similar to Pacific–South America (PSA) patterns (Mo and Higgins 1998; Mo and Nogés-Paegle 2001). When significant, an upper-level cyclonic intraseasonal anomaly over South America interacts with eastward propagating synoptic disturbances and strengthens the cyclonic flow in the surroundings of the subtropical jet, leading to heavy rainfall. It is suggested that the subtropical cyclonic perturbation described by Vera and Vighiarolo (2000) is linked to the intraseasonal anomalies observed here. Therefore, the design of a prediction scheme to forecast extreme precipitation events with more than a week in advance should closely follow the development of intraseasonal anomalies in the tropics, consequent teleconnections and the development of intraseasonal anomalies flanking the South American subtropical jet.

The paper is organized as follows: Sect. 2 introduces the dataset and methods. These are the same as those in Hirata and Grimm (2015). Sections 3, 4, and 5 describe the life cycles of rainfall extremes during spring, fall, and winter, respectively. The influence of large scale tropical convection (such as that associated with the MJO) is inspected in Sect. 6, followed by a summary of the results and discussion in Sect. 7.

2 Data and methods

The datasets and methods are the same used in Hirata and Grimm (2015). The Climate Prediction Center (CPC) Unified Gauge-Based Analysis of Global Daily Precipitation dataset on a horizontal grid of 0.5° resolution (Chen et al. 2008) and NCEP reanalysis data (Kalnay et al. 1996), on a horizontal grid of 2.5° , are used to define precipitation extremes and to characterize their synoptic and intraseasonal evolution, from 1979 to 2013.

An extreme precipitation event is defined whenever the area-averaged daily rainfall rate exceeds the 95th percentile

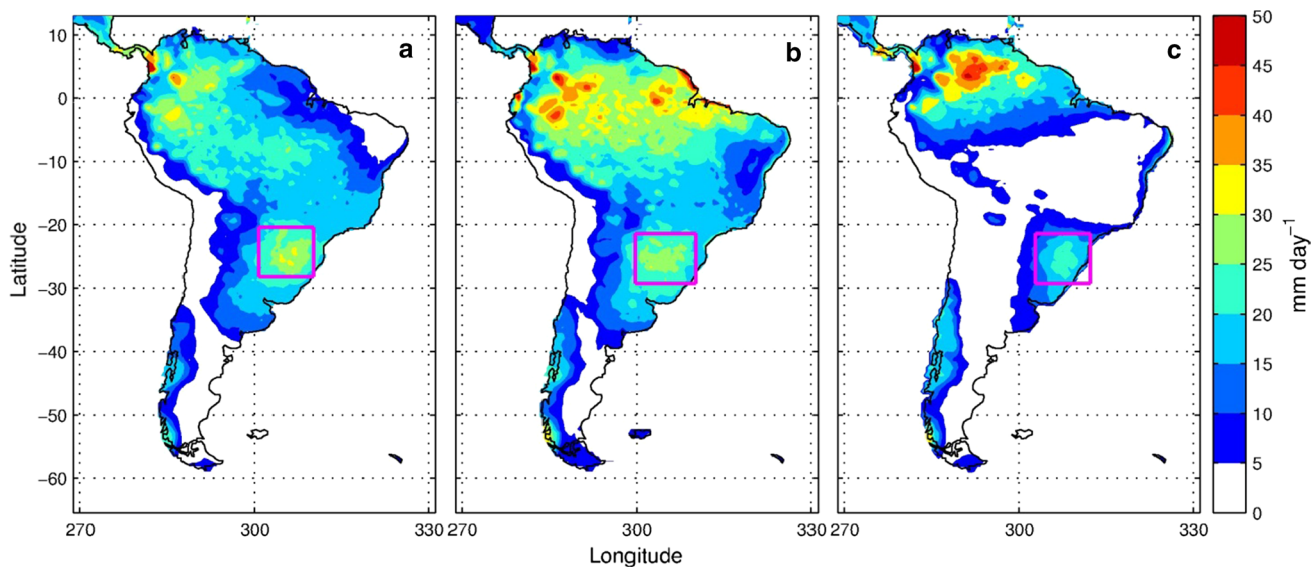


Fig. 1 The 95th rainfall percentile for **a** spring, **b** fall and **c** winter. The *magenta box* indicates the location of the region with highest value of the 95th percentile over southeastern South America

during each season, for at least 1 day. There are different 95th percentiles for the spring, fall and winter. Figure 1 displays the value of the 95th precipitation percentile in South America for each grid point, using the CPC dataset. The boxes indicate the regions with highest value of the 95th percentile of daily precipitation south of the Amazon, and are used to produce the area-averaged daily rainfall series. Although the definition of each region is rather arbitrary, variations of the method used to estimate it do not change the results.

Anomaly composites are calculated for extreme events in each season, from 5 days before until the day of maximum rainfall but only days -4, -2 and the day of the event are displayed in the figures. The significance is assessed by a bootstrap technique with 1000 iterations (Livezey and Chen 1983). Winds are considered significant only when the wind speed is significant. As in Hirata and Grimm (2015), the number of events exceeding the 95th percentile varies from season to season because the analysis excluded days with area-averaged precipitation below 1 mm day^{-1} . In the composite cycle, composite day 0 is the day of maximum area-averaged rainfall.

A band-pass Lanczos filter is used to split geopotential height anomalies in two frequency bands: a synoptic (3–10 days) and an intraseasonal (20–90 days). The same filtering technique is applied on outgoing longwave radiation (OLR) (Liebmann and Smith 1996) anomalies to retain the intraseasonal signal. Historical El Niño and La Niña conditions are taken from the CPC definition based on the Oceanic Niño Index (ONI). Warm and cold episodes are defined when a three month running mean anomaly

exceeding $\pm 0.5 \text{ }^\circ\text{C}$ for at least five consecutive months in the Niño 3.4 region is identified. The total number of days under each ENSO phase was calculated by adding the days between the first day of the month in which each ENSO event started and the last day of the month in which each event ended.

The all-season real-time multivariate MJO index (RMM) (Wheeler and Hendon 2004) is used to relate the occurrence of rainfall extremes to the location of large scale tropical intraseasonal convection. It is important to note that we use the 8 phases of the RMM index as an indication of the location of tropical convection, independent of its eastward propagation. Therefore, the analysis is not restricted to MJO events with coherent propagation. Instead, our study aims to verify if tropical convection along the tropical belt has played a role in the evolution of extreme rainfall events over South America.

3 Spring (SON)

In spring, the region with the highest 95th percentile of area-averaged daily precipitation south of the Amazon is observed over southeastern South America (subtropical La Plata Basin, Fig. 1a). The region also exhibits the highest number of extreme events when compared to the other seasons analyzed here (Table 1) and the highest value of the 95th percentile (area average of $16.94 \text{ mm day}^{-1}$).

Close to the surface, the synoptic life cycle of spring-time extreme rainfall events under neutral ENSO conditions begins with negative sea level pressure (SLP)

Table 1 Number of identified rainfall extreme events (>95th percentile) per season and ENSO phase, the percentage of extremes relative to the total number of extremes, the approximate number of days under each ENSO phase and the percentage of extremes relative to the number of days under each ENSO phase

Spring (SON)	Number of events	%	Number of days from 1979 to 2013	Relative frequency (%)
El Niño	44	33.6	819	5.4
La Niña	33	25.2	970	3.4
Neutral ENSO	54	41.2	1396	3.9
Total	131	100	3185	4.1
<i>Fall (MAM)</i>				
El Niño	27	24.1	522	5.1
La Niña	22	19.6	707	3.1
Neutral ENSO	63	56.3	1991	3.2
Total	112	100	3220	3.5
<i>Winter (JJA)</i>				
El Niño	33	29.2	675	4.9
La Niña	15	13.3	553	2.7
Neutral ENSO	65	57.5	1992	3.3
Total	113	100	3220	3.5

The number of days under each ENSO phase is estimated using ONI data taken from the CPC web site, considering the first day of the month in which the event begins and the last day of the month in which it ends as determined by the CPC (www.cpc.ncep.noaa.gov/products/analysis_monitoring/ensostuff/enso-years.shtml)

anomalies crossing the Andes south of 25°S around four to 5 days before maximum rainfall (Fig. 2a). The anomalies move northward in the next couple of days, reaching tropical latitudes (Fig. 2b). At the day of the event, a cyclonic anomaly is centered over the Uruguayan coast, with significant northwesterly winds blowing from southern Amazon toward the Brazilian coast (Fig. 2c). Significant negative SLP anomalies extend over the Amazon basin and into the Northern Hemisphere. Positive SLP anomalies are present to the east of the Andes south of 25°S (Fig. 2c). The lower atmosphere is anomalously warmer near the cyclonic anomaly, accompanied by strong upward motion in the midlevels to the northeast of a sharp gradient of 1000–500 thickness anomalies (which indicates the approximate position of the front) and downward motion to the southwest of the front (Fig. 3a–c).

In the upper-levels, there is a high-frequency wave train intensifying and moving eastward from the central Pacific to South America (Fig. 4a–c). Intraseasonal anomalies are stronger near the South American subtropical jet axis after composite day-3 (Fig. 4b, c) and the combination of both signals indicates that the anomalies favor southward moisture transport from the tropics to the subtropics during the development of the extreme event. It is important to note the presence of negative geopotential height anomalies in the intraseasonal band to the south of the subtropical jet in the Pacific and over South America.

In the Pacific, the anomalies seem to originate from around the subtropical jet exit, where the deceleration of the zonal winds is stronger, favoring wave energy accumulation and consequent emanation according to theoretical

arguments (Webster and Chang 1988). Apparently, synoptic anomalies grow and propagate eastward from that location. On the other hand, negative intraseasonal height anomalies south of the jet may indicate an acceleration of the jet, which would imply in less potential for wave energy accumulation in the region. However, even with the acceleration of the jet by the cyclonic anomaly around its exit, it is clear that the magnitude of the climatological zonal winds in the region still supports an area of negative zonal stretching deformation and wave accumulation in the South Pacific.

Over South America, the center of negative intraseasonal height anomalies south of the jet grows as the synoptic wave moves eastward. A center of positive intraseasonal height anomalies becomes significant and also grows northeast of the subtropical jet 2 days before maximum rainfall (Fig. 4b) indicating an evolution of the intraseasonal anomalies. It is possible that the events, in this case, occur as a result of a combination of two waves, one synoptic and one intraseasonal. The anomalous pair of positive geopotential anomalies to the northeast and negative anomalies to the southwest of the jet axis indicates an acceleration of the jet over the region (and its undulation), favoring ascending motion east of the through (Fig. 3c), and less potential for wave energy accumulation and convective activity in the SACZ region, as also reported for the austral summer (Hirata and Grimm 2015). Less convective activity over the SACZ also favors excessive precipitation in the focused region.

The evolution of these extremes during El Niño years close to the surface is very similar (Fig. 2e, f), but the upper-levels indicate that the intraseasonal signal is barely significant (Fig. 4d–f). Under La Niña conditions (Fig. 4g–i), the

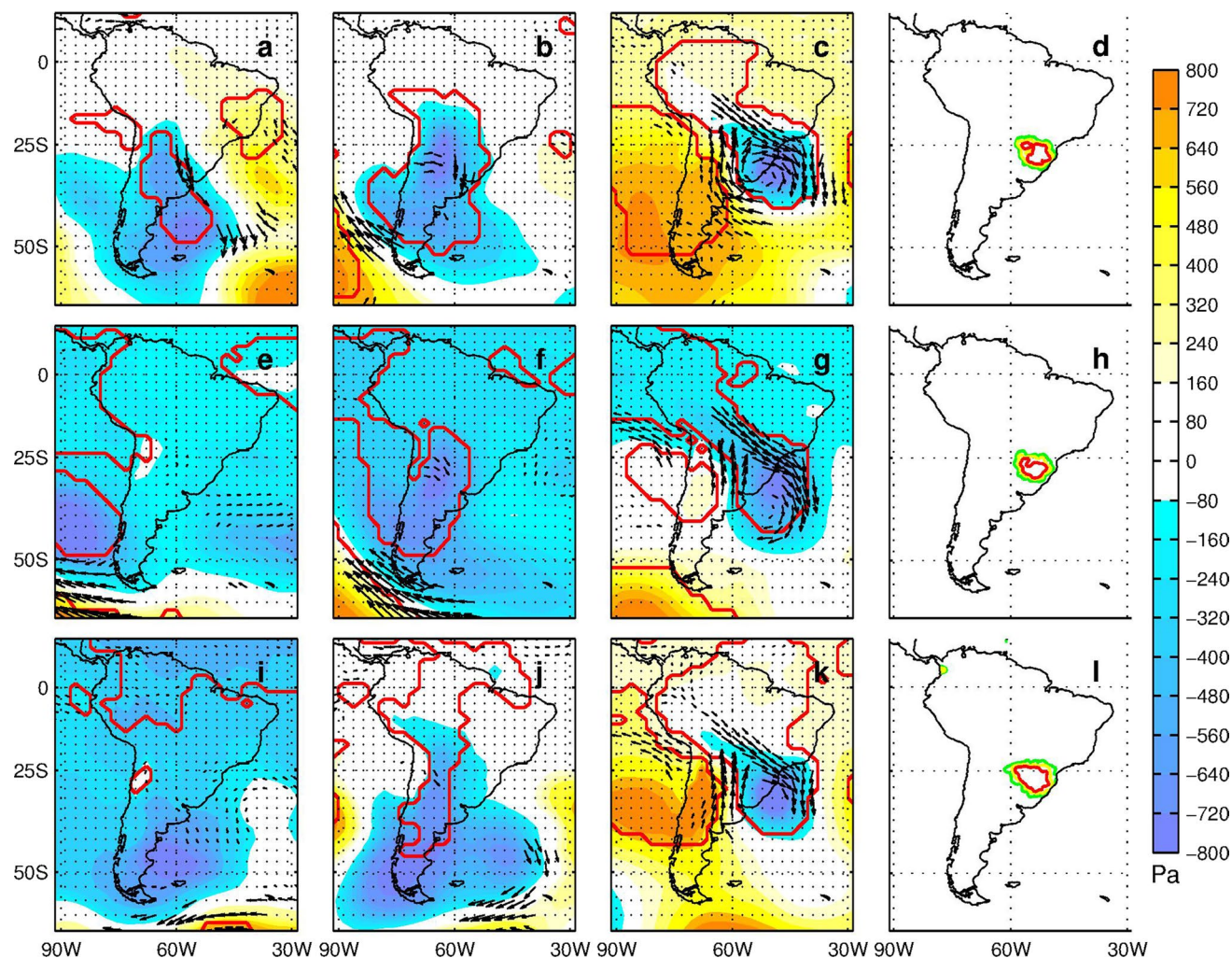


Fig. 2 Composites (days-4, -2 and 0) of extreme rainfall synoptic evolution over southeastern South America during spring. **a–c** Neutral ENSO conditions, **e–g** El Niño conditions, and **i–k** La Niña conditions. Shading represents SLP anomalies, arrows represent 850 hPa wind vectors (only vectors significant at 95 % are plotted), and red

contours represent SLP significance (95 %). (**d, h, l**) Display the area-averaged 95th percentile rainfall rate (green), the 95th percentile +5 mm day⁻¹ (yellow), and the 95th percentile +10 mm day⁻¹ (red) on composite day 0 for Neutral ENSO, El Niño and La Niña conditions, respectively

intraseasonal signal in the upper troposphere is significant but both frequency bands exhibit weaker anomalies compared to the cases under neutral ENSO conditions. Intraseasonal anomalies are significant flanking the South American subtropical jet and also grow with the approach of the synoptic anomalies. The origin of these intraseasonal anomalies is uncertain, especially due to the lack of significance of any intraseasonal signal in the Pacific basin.

El Niño seasons exhibit an increased relative frequency of rainfall extremes apparently due to synoptic activity, since intraseasonal anomalies are less significant (Table 1). The relative frequency of rainfall extremes drops during neutral ENSO and La Niña conditions, when the interaction of synoptic and intraseasonal anomalies is more important to drive moisture from the Amazon.

4 Fall (MAM)

Extreme precipitation events in the fall affect a region located slightly to the south of the spring box (Fig. 1b). A total of 112 extreme events are identified (Table 1) with an area-averaged 95th percentile of 15.91 mm day⁻¹.

Composites of low level winds and SLP anomalies indicate that the synoptic evolution of rainfall extremes is similar to springtime events although negative SLP anomalies seem to originate from extratropical anomalies in the Atlantic sector (Fig. 5a–c). Low level circulation intensifies when positive SLP anomalies enter the continent near 50°S and negative anomalies strengthen over the Chaco region. At the day of the event, the low level cyclone is fully formed, fueled by moisture transported southward

Fig. 3 Same as Fig. 2 but the shading now represents 1000–500 hPa thickness anomalies for **a–c** Neutral ENSO, **d–f** El Niño, and **g–i** La Niña conditions. *Red contours* indicate significant thickness anomalies at 95 % level. *Black solid (dashed) contours* represent positive (negative) 500 hPa omega anomalies at 0.02 Pa s⁻¹ intervals. Only significant omega anomalies are plotted

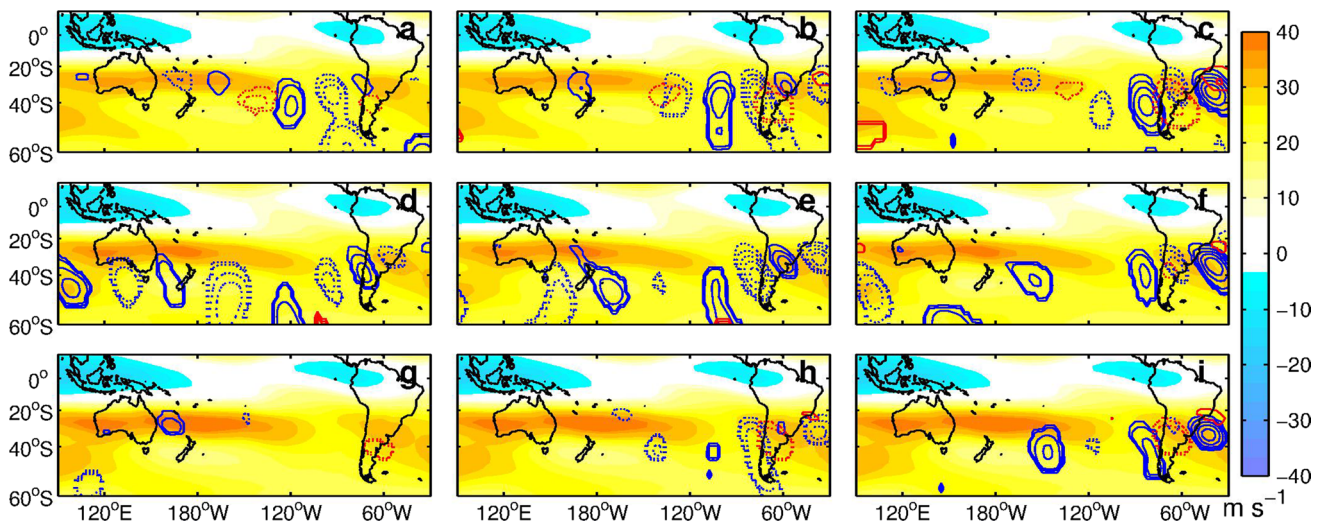
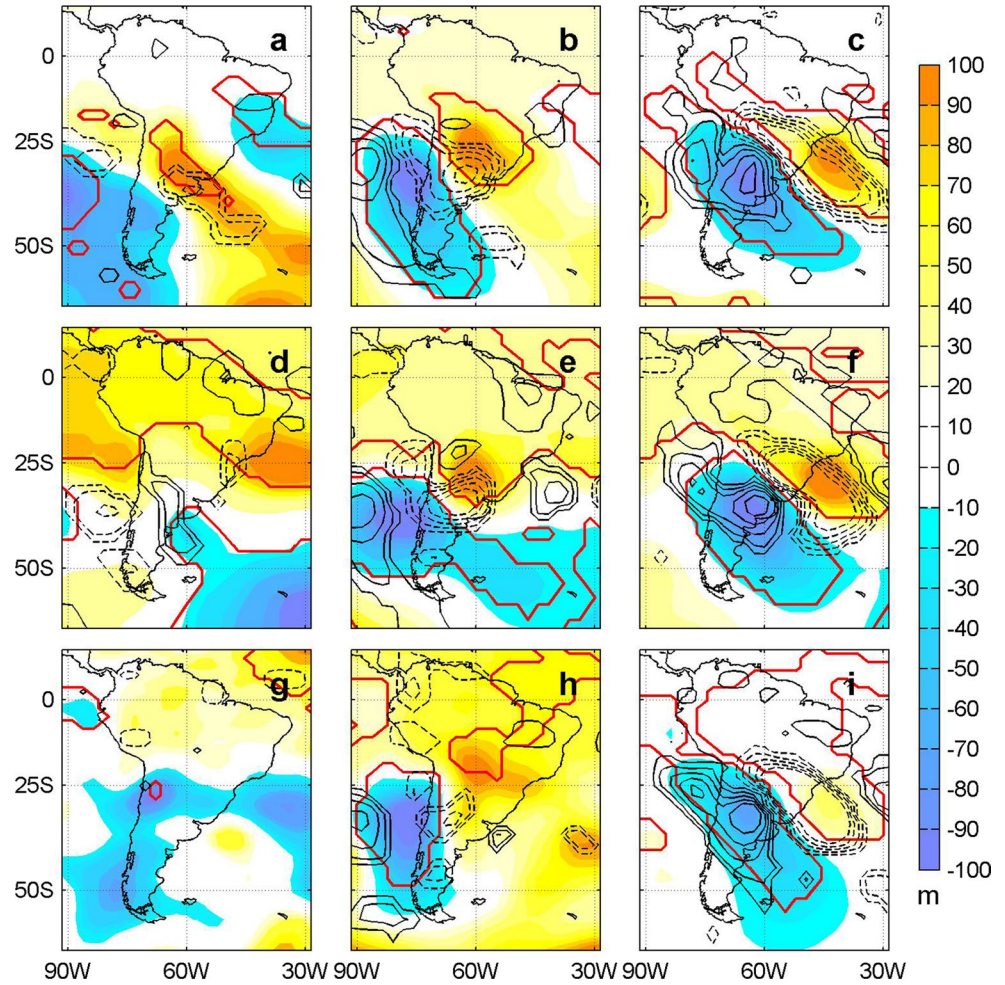


Fig. 4 Same as Fig. 3 but shading now represents climatological 200 hPa zonal winds for **a–c** Neutral ENSO, **d–f** El Niño, and **g–i** La Niña conditions. *Contours* represent filtered 3–10-(blue) and 20–90-

day (red) 200 hPa geopotential height anomalies at 10 m intervals, with *solid (dashed) contours* indicating positive (negative) anomalies. Only significant anomalies are plotted

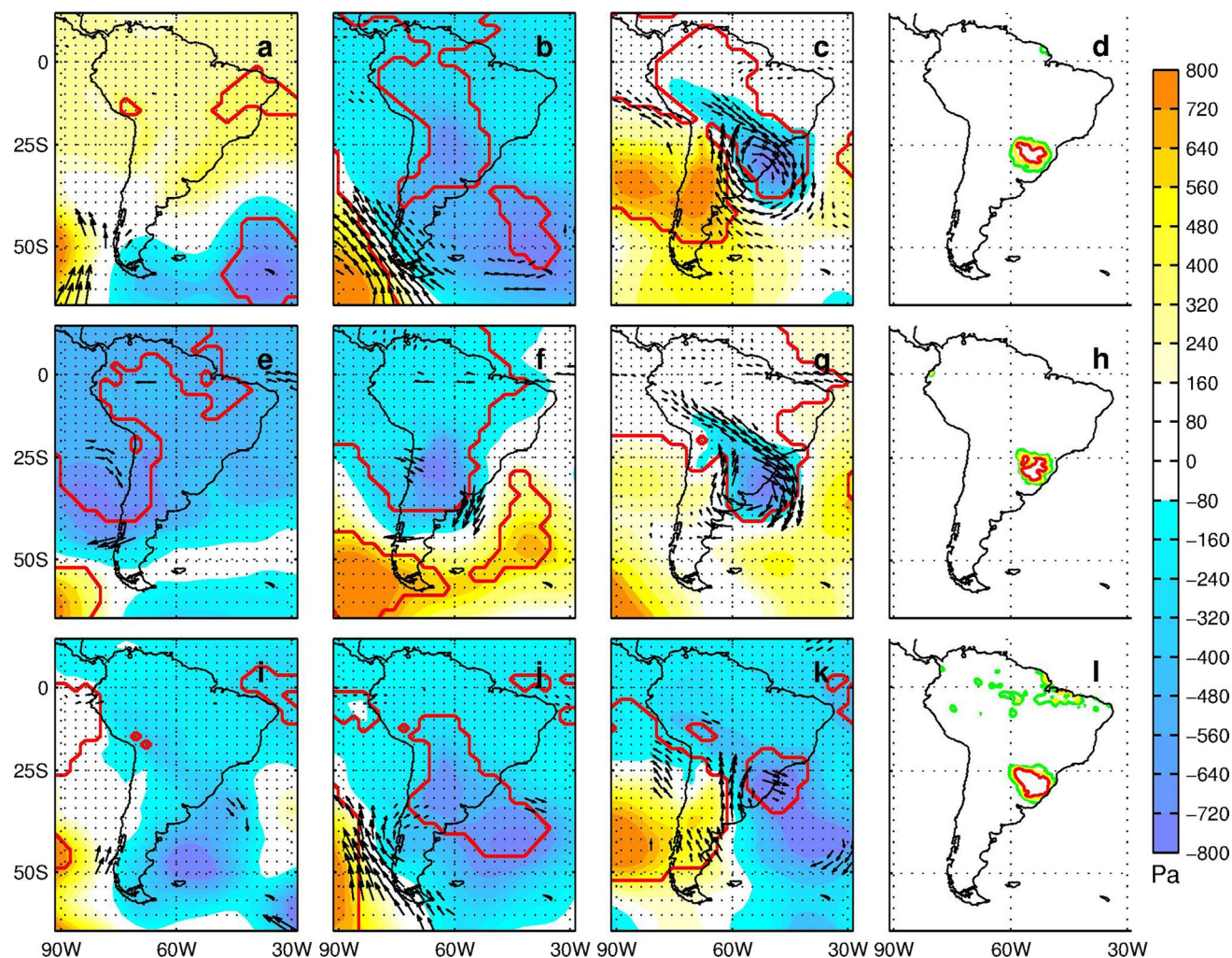


Fig. 5 Same as Fig. 2 but for fall (MAM)

from the Amazon (Fig. 5c). The lower troposphere north of 25°S is significantly warmer than average during the life cycle of these events (Fig. 6a–c). Two days before the precipitation maximum (Fig. 6c), an area of cold air begins to propagate northeastward. Intense upward motion leads the cold air propagation while subsidence follows to the southwest.

In the upper-levels, an anomalous high-frequency wave train is observed extending from the Pacific to southeastern South America and propagating eastward while intraseasonal anomalies stand east of 120°W (Fig. 7a–c). The resulting wave is a combination of strong intraseasonal and synoptic anomalies. While the intraseasonal anomalies are apparently stationary (due to their relatively longer period), the synoptic signal propagates eastward. At the day of the extreme (Fig. 7c), the anomalies are aligned around the subtropical jet over South America, favoring southward moisture transport from the Amazon. In this situation, the large center of positive intraseasonal anomalies near the

subtropical jet exit in the Pacific indicates a deceleration of zonal winds on its northern side, in accordance to the arguments of wave energy accumulation proposed by Webster and Chang (1988). In this case, the intraseasonal wave appears to interact with the incoming synoptic anomalies just before maximum rainfall.

Extremes are relatively more frequent with El Niño conditions (Table 1). Rainfall extremes under El Niño conditions are related to low level negative SLP anomalies crossing the Andes south of 25°S (Fig. 5e–g), cyclonic anomalies and a well-established low level jet east of the Andes (Fig. 5g). However, intraseasonal anomalies are not significant in the upper-levels at the day of the event under El Niños (Fig. 7f). On the other hand, under La Niña conditions, the anomalous pattern is less significant in the lower-levels (Fig. 5i–k) even though it is very similar to the cycle under neutral ENSO conditions. Moreover, the area under heavy rainfall is slightly larger during La Niña events than during other ENSO phases (Fig. 5l). Intense intraseasonal

Fig. 6 Same as Fig. 3 but for fall (MAM)

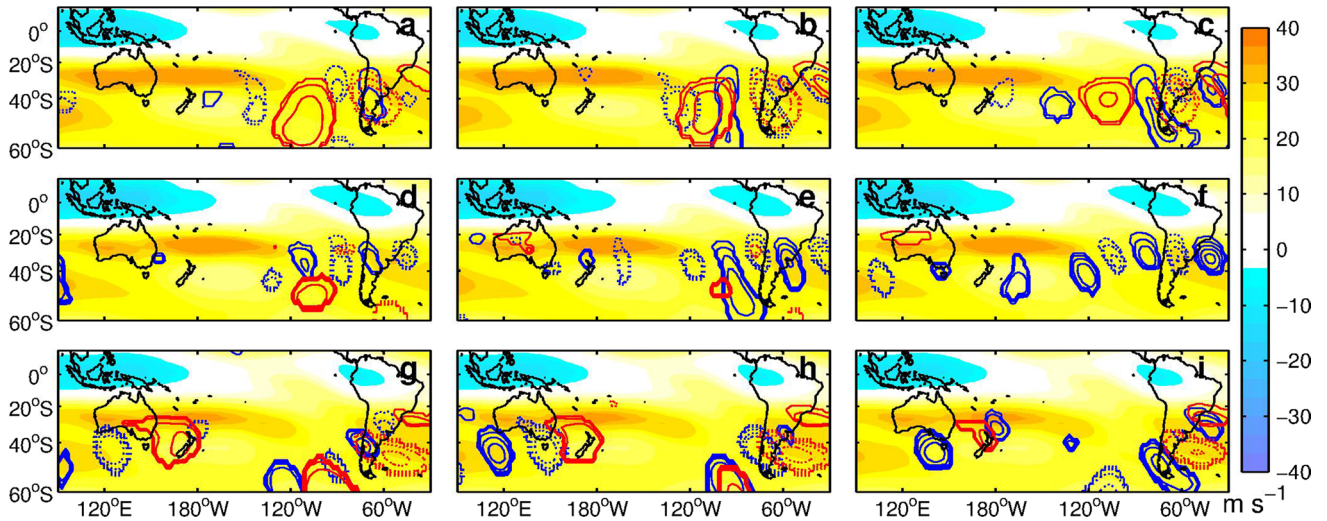
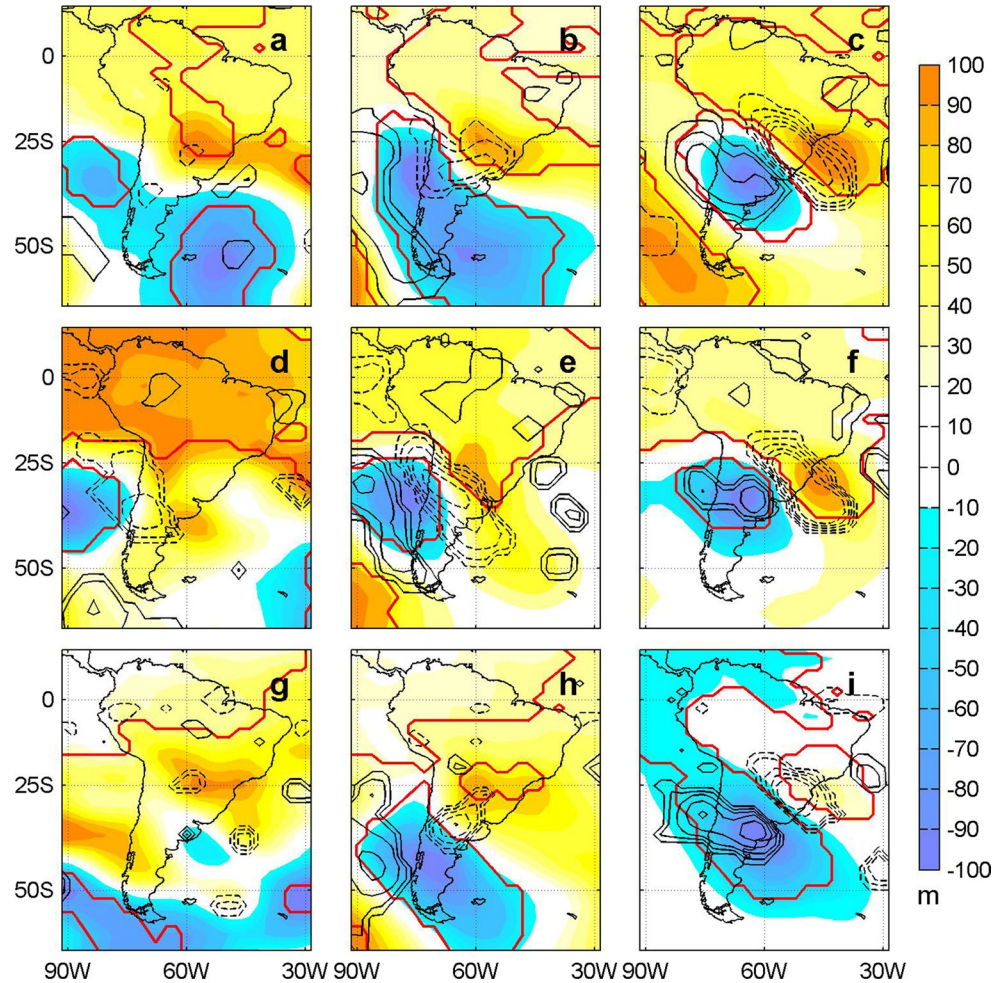


Fig. 7 Same as Fig. 4 but for fall (MAM)

and synoptic anomalies are observed in the upper-levels with wave-like signals coming from the subpolar region (Fig. 7g–i). As in the spring, the geopotential anomalies

around the South American subtropical jet indicate an acceleration of the jet and less potential for wave accumulation in the SACZ region, with the interaction of the

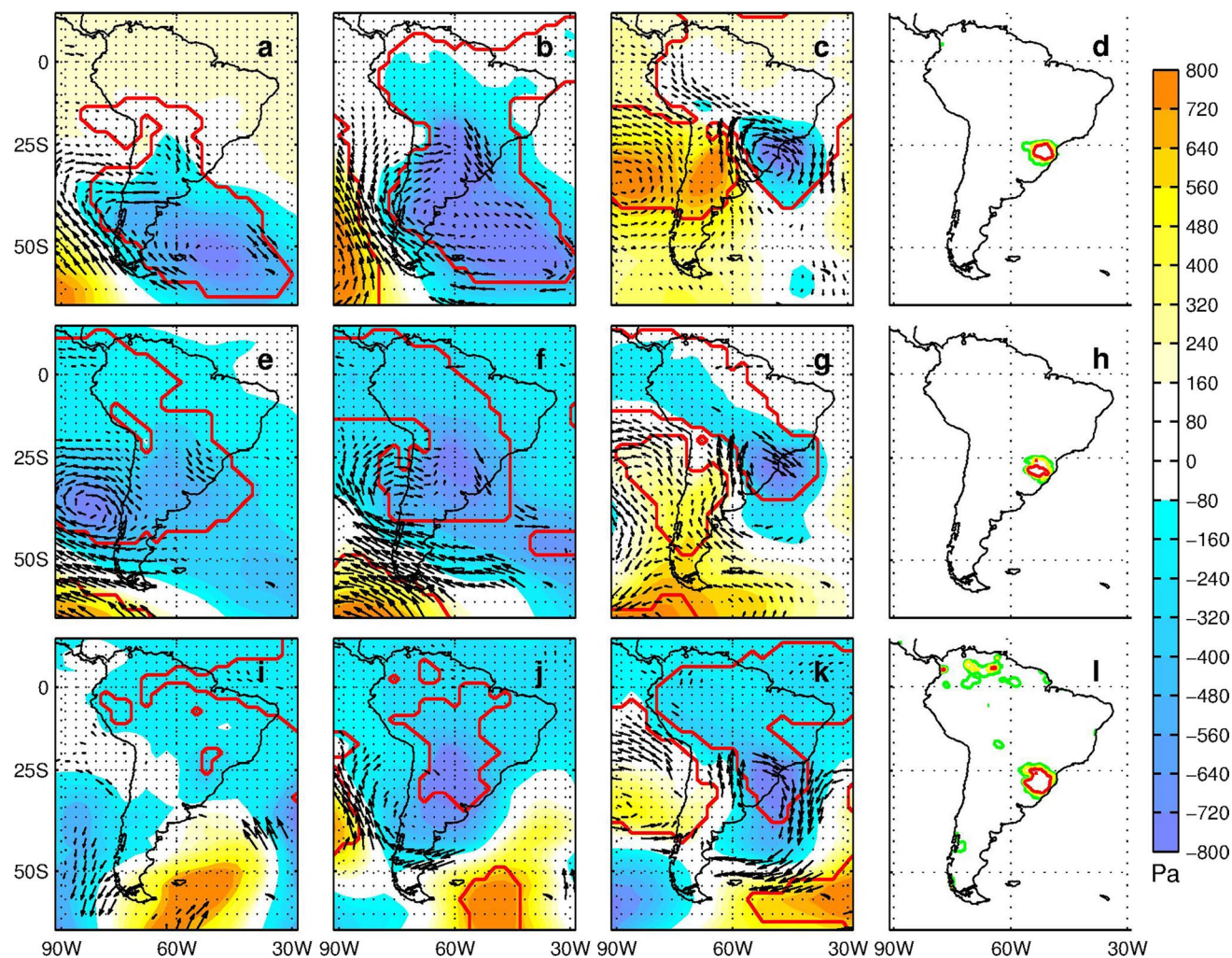


Fig. 8 Same as Fig. 2 but for winter (JJA)

synoptic with the intraseasonal wave favoring the occurrence of the rainfall extreme.

5 Winter (JJA)

The region south of the Amazon most affected by heavy rainfall is still over southeastern South America, now closer to the coast (Fig. 1c). The area-averaged 95th percentile is the smallest ($13.79 \text{ mm day}^{-1}$) among the seasons, and events exceeding the 95th percentile were observed 113 times (Table 1).

Once again, the life cycle of extremes is related to the passage of a frontal system to the east of the Andes (Fig. 8). Near the surface, an anomalous low pressure center south of 25°S is observed over the southeastern South American coast. Negative SLP anomalies extend northward over the continent while positive SLP anomalies strengthen over the southeast Pacific (Fig. 8c, g, k). During neutral ENSO

conditions, once positive SLP anomalies move eastward crossing the Andes, a southerly flow becomes significant to the east of the mountains and northwesterly low-level flow from tropical latitudes brings moisture to fuel convection over southern Brazil and Uruguay (Fig. 8c).

The evolution of the disturbance in the lower troposphere is similar to that observed in spring and fall, with the growth of a significant warm region over southern Brazil and Uruguay, and the northeastward propagation of cold anomalies associated with the surface anticyclone (Fig. 9). At this point, intense upward motion occurs on the leading edge of the cold anomalies and strong subsidence to the southwest intensifies the cold anticyclonic anomalies moving equatorward.

In the upper troposphere during neutral ENSO conditions, geopotential height anomalies highlight an intraseasonal wave pattern extending from the Pacific into South America, consistent with Rossby wave dispersion on a sphere (Fig. 10a–c). The separation of the anomalies in

Fig. 9 Same as Fig. 3 but winter (JJA)

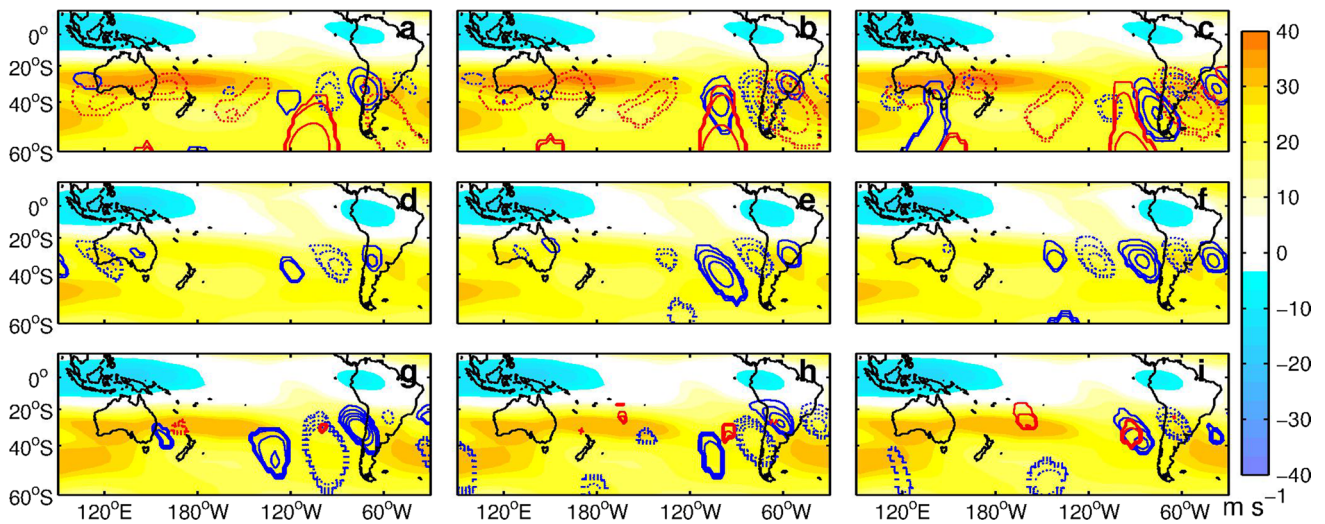
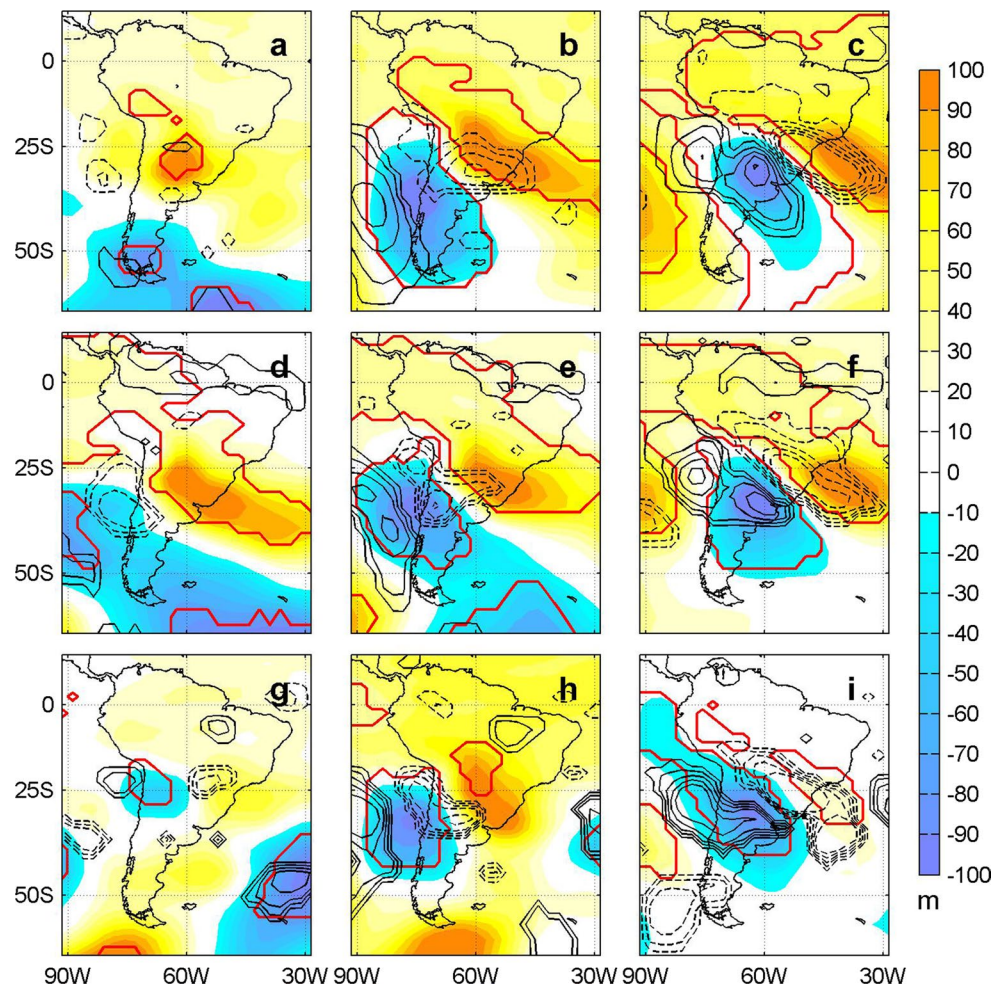


Fig. 10 Same as Fig. 4 but for winter (JJA)

two frequency bands indicates that both synoptic and intra-seasonal signals are significant components of a propagating wave. Particularly, it is important to note negative

geopotential height anomalies indicating anomalous cyclonic flow over the subtropical jet in South America at the day of maximum rainfall (Fig. 10c). Under El Niño

cases, only synoptic anomalies are significant in the upper troposphere, with intraseasonal anomalies losing significance completely (Fig. 10d–f). Under La Niña conditions, the surface cyclone apparently moves eastward from the Pacific, but the southerly and the northwesterly flow are less significant (Fig. 8k). In the upper-levels (Fig. 10g–i), the significance of intraseasonal anomalies sharply decreases compared to neutral ENSO cases around the South American subtropical jet.

6 Links with tropical intraseasonal convection

During summer, around 38 % (31 out of 81) of rainfall extremes in the SACZ are preceded by RMM index on phases 6 and 7 around 10 days before the event, indicating that large scale intraseasonal convection is located somewhere between the Maritime Continent and the western Pacific (Hirata and Grimm 2015). Considering a 40-day intraseasonal cycle, each phase would last for 5 days and thus maximum summer rainfall in the SACZ would occur around phases 8 and 1, when the anomalous convection is over the central tropical and southern subtropical Pacific. This is the most robust relationship between the RMM index and rainfall extremes in southeastern South America.

As in summer, during non-summer conditions intraseasonal anomalies are significant under neutral ENSO and La Niña phases. However, the preferred RMM index phase preceding maximum rainfall in southeastern South America and the lead-lag relationship varies from season to season. In spring, intraseasonal anomalies are significant during both neutral ENSO and La Niña conditions. Figure 11 displays the distribution of RMM index phase 10 days before the springtime 54 rainfall extremes identified under neutral ENSO conditions. Nearly half of these events (25, or 46 %) occurred with the RMM index on phases 1 or 2 about 10 days before maximum rainfall (Fig. 11). The significance of the distribution displayed in Fig. 11 was assessed using a Chi square test for categorical data at 5 % significance level:

$$\chi_c^2 = \sum \frac{(O_i - E_i)^2}{E_i}$$

where χ_c^2 is the calculated Chi square statistic to be compared with the tabled data, O_i is the observed value of extreme events preceded by each RMM phase and E_i is the expected value. The test assumed that the null hypothesis is that the occurrence of an extreme rainfall event is independent of the RMM index phase (i.e., South America extreme rainfall events are independent of the location of tropical intraseasonal convection). In this case, expected occurrence of an extreme is the same for any given phase of the index. In spring under neutral ENSO years, this expected value is

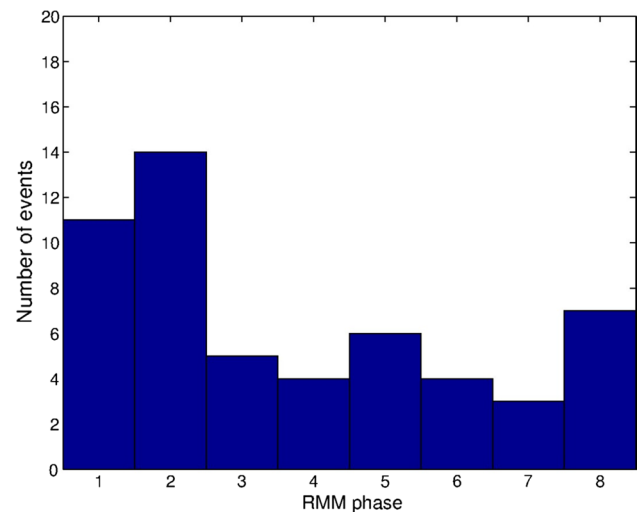


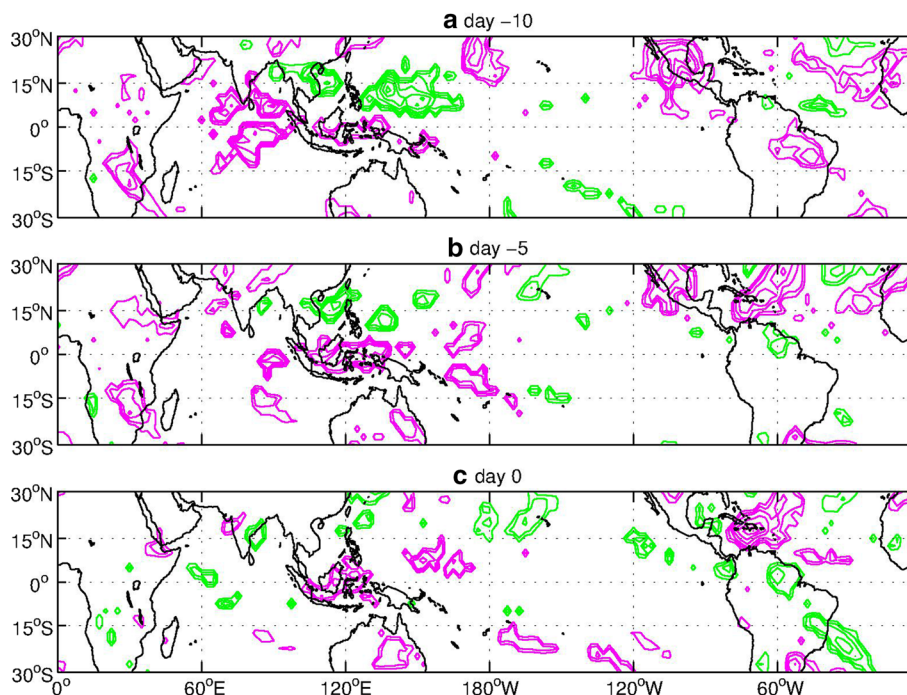
Fig. 11 RMM index phase 10 days before extreme events in southeastern South America during spring (SON) under neutral ENSO conditions

6.75 events for each RMM phase. The number of degrees of freedom in this particular case is 7 (the number of RMM phases minus 1). The test rejected the null hypothesis for the extreme events during the spring, under neutral ENSO conditions. This means that only in spring and under neutral ENSO conditions, the occurrence of extreme events in South America is not independent on the location of tropical convection as defined by the RMM index.

If the RMM index in phases 1 or 2 is predominant about 10 days before maximum rainfall in southeastern South America during neutral ENSO springs, the intraseasonal anomalous convection is located somewhere between the central Indian Ocean and the Maritime Continent, with anomalous subsidence over the central tropical/subtropical southern Pacific. Therefore, extremes would occur mostly around phases 3 and 4. Figure 12 shows filtered OLR composites for springtime extreme events under neutral ENSO conditions and RMM amplitude larger than 1, to select only cases when intense tropical convective activity 10 days before maximum rainfall over the target area is observed. These intense convection associated with the MJO correspond to 29 out of the 54 events (53 %). As expected, significant negative anomalies are observed over the Indian Ocean 10 days before the extremes (Fig. 12a). Five days later, the intraseasonal convective signal is over the Maritime Continent (Fig. 12b).

Figure 4a–c indicate the presence of an upper-level synoptic wave train over the Pacific basin, significant eastward of the dateline and with a center of significant negative 200 hPa geopotential height intraseasonal anomalies located over the southern subtropical Pacific, around 30°S, and other intraseasonal anomalies developing eastward,

Fig. 12 Band-passed filtered OLR anomaly composites for extreme events in spring under neutral ENSO conditions and RMM amplitude larger than 1 at **a** day -10, **b** day -5, and **c** day 0 (rainfall maximum in South America). *Magenta* (*green*) indicates negative (positive) OLR anomalies. Contour interval is 1.5 W m^{-2} . Zero line is omitted. Only 95 % significant anomalies are plotted



over South America (Fig. 4a–c), consistent with the intraseasonal teleconnection between central Pacific and South America, proposed by Grimm and Silva Dias (1995), based on influence function analysis. There may be some influence of the tropical convective activity over the Maritime Continent related with the MJO on the synoptic wave train carrying the high-frequency component eastward (Fig. 4a–c). With the presence of intraseasonal anomalies over South America, the occasional passage of a high-frequency disturbance amplifies the anomalies and facilitates the occurrence of extreme rainfall.

During La Niñas, the best relationship between the RMM index and rainfall extremes in spring is observed when tropical intraseasonal convection tends to occur over the Maritime Continent or western Pacific (phases 5 and 6) 15 days before maximum rainfall over South America, in 15 out of 33 events (45 %). Even though the ratio of extremes preceded by phases 5 and 6 reaches almost 50 % of the events in this category, the Chi square test for categorical data does not reject the null hypothesis of independence between the RMM phase and the occurrence of extremes. Upper-level anomalies indicate significant signals in the extratropics from the Pacific to South America (Fig. 4g–i), and the lead-lag relationship suggests that extreme rainfall in southeastern South America coincides with tropical convection over the western hemisphere (phases 8 or 1, considering 5-day RMM phases). Low-level composites (Fig. 2i–k) show significant negative SLP anomalies in the tropics a few days before the rainfall extremes, suggesting a tropical link between the occurrence of rainfall extremes and the

global intraseasonal cycle. However, the non-significance of the Chi square test indicates that a larger sample size may be needed to confirm the hypothesis that extremes in southeastern South America during spring of La Niñas are associated with large scale tropical convection on RMM phases 8 or 1.

In fall, the combination of synoptic and intraseasonal anomalies is also important during neutral ENSO and La Niña conditions. However, the Chi square test of categorical data does not reject the null hypothesis of independence between the occurrence of extremes and the RMM phase. As in the spring, the 200 hPa geopotential height intraseasonal anomalies during neutral ENSO conditions are significant eastward of the dateline, and upper-level synoptic anomalies are present near New Zealand (Fig. 7a–c). It is important to note that a few days before maximum rainfall in southeastern South America, the intraseasonal signal appears nearly as a standing oscillation due to its longer period. Meanwhile, synoptic waves regularly traveling eastward occasionally match their centers of action with the intraseasonal ones, intensifying the signal and favoring the occurrence of heavy rainfall over southeastern South America.

Under La Niña conditions, the relationship between the RMM index phase and rainfall extremes in southeastern South America is not clear but wave-like signals are observed in the extratropics (Fig. 7g–i). Both synoptic and intraseasonal anomalies are important. In the southeastern Pacific and South American sector, the band-passed anomalies indicate that wave-like disturbances on both synoptic

and intraseasonal frequencies come from high latitudes, suggesting long Rossby wave dispersion rays. A striking feature of these composites is the center of positive intraseasonal anomalies over New Zealand, just poleward of the subtropical jet axis east of Australia, suggesting a deceleration of the zonal winds. It is possible that the deceleration of the upper-level winds induces wave accumulation and emanation from the surroundings of the SPCZ, triggering the long wave train reaching South America favoring rainfall extremes.

Winter is a season when intraseasonal anomalies are important only under neutral ENSO conditions (Fig. 10a–c). RMM index on phases 5 and 6 lead extreme rainfall over southeastern South America by 10 days in 24 out of 65 (37 %) identified events. This indicates tropical convection over the western Pacific or the Western Hemisphere as the extreme event in South America approaches. However, the Chi square test does not reject the null hypothesis of independence. On the other hand, intraseasonal anomalies during the life cycle of winter extremes are the strongest, with a well-defined upper-level wave train extending from the central Pacific to the South American sector (Fig. 10a–c). Rossby wave propagation resulting from tropical divergent forcing is favored within the range of westerlies in the winter hemisphere (Hoskins and Ambrizzi 1993; Berbery et al. 1992). The divergent forcing, in these cases, may be also located somewhere in the western/central Pacific, as indicated by the upper-level composites (Fig. 10a–c). Strong synoptic anomalies are also observed during the wintertime life cycle.

7 Summary and discussion

During non-summer conditions, extreme rainfall impacts on densely populated areas south of the Amazon are concentrated in southeastern South America, in a region whose limits change little from season to season. Rainfall extremes during non-summer conditions over this region are mainly driven by synoptic disturbances propagating equatorward east of the Andes. Depending on the ENSO phase during each particular season, intraseasonal anomalies are instrumental in the evolution of these extreme events. Significant relatively persistent intraseasonal anomalies around the continent are observed during neutral ENSO conditions of all seasons and during the spring and fall of La Niñas. During neutral ENSO conditions, these intraseasonal anomalies seem to originate in the central subtropical southern Pacific. The most robust relationship between South American extreme rainfall events and large scale tropical intraseasonal convection is observed in spring under neutral ENSO conditions. Extremes are apparently favored by tropical convection somewhere between the central/eastern Indian

Ocean and the Maritime continent and subsidence in the central tropical/subtropical southern Pacific. This signal is significant when the RMM amplitude is larger than 1 and on phases 1 and 2 around 10 days before maximum rainfall over the target area.

The rainfall extremes described here exhibit the characteristics of strong frontal systems penetrating the low latitudes of South America to the east of the Andes (Marengo et al. 1997; Vera and Vigliarolo 2000). Vera and Vigliarolo (2000) proposed a mechanism for the generation of strong wintertime cold air outbreaks in South America, east of the Andes: an interaction between a subpolar cyclonic perturbation moving equatorward with an upper-level eastward moving cyclonic perturbation at subtropical latitudes. Our results indicate that intense negative upper-level geopotential height anomalies, part of a long extratropical wave train, act over the continental subtropics during the development of extreme rainfall events over southeastern South America. This cyclonic anomaly is a result of the combination of synoptic and intraseasonal anomalies. Synoptic disturbances are observed moving mostly eastward while intraseasonal anomalies exhibit a more meridional structure due to the equatorward veering after the Andes Cordillera, in agreement with Rossby wave dispersion on a sphere (Hoskins and Ambrizzi 1993) and PSA modes (Mo and Higgins 1998). Therefore, it seems that the upper-level cyclonic anomaly is associated with the intraseasonal cycle during neutral ENSO, and spring and fall of La Niñas.

The increased frequency of rainfall extremes under El Niño conditions is independent of intraseasonal anomalies. The source of moisture for the extremes is located in tropical South America and this moisture is transported southward by a northwest-southeast flow similar to the low-level jet east of the Andes. Under El Niño conditions, suppression of South American tropical convection by the anomalous Walker circulation diverts moisture southward. Enhanced moisture transport into southeastern South America is associated with warm ENSO conditions, especially the eastern (canonical) El Niño (Tedeschi et al. 2015). Occasional passage of synoptic disturbances then are able to tap the moisture flow, facilitating the occurrence of rainfall extremes over the target region, as in Liebmann et al. (2004).

Intraseasonal anomalies flanking the South American subtropical jet during extreme events in southeastern South America usually indicate an acceleration of the jet and consequently less potential for wave energy accumulation in the SACZ. While the interaction of synoptic and intraseasonal signals is often sufficient for the occurrence of an extreme event in southeastern South America, wave accumulation is important for heavy rainfall in the SACZ (Hirata and Grimm, 2015).

Acknowledgments This work was carried out with the support of the National Council for Scientific and Technological Development (CNPq-Brazil) Grant BJT 400547/2013-9, and with the aid of the Inter-American Institute for Global Change Research (IAI) Grant CRN3035, which is supported by the US National Science Foundation (Grant GEO-1128040).

References

- Alvarez MS, Vera CS, Kiladis GN, Liebmann B (2015) Influence of the Madden–Julian oscillation on precipitation and surface air temperature in South America. *Clim Dyn*. doi:[10.1007/s00382-015-2581-6](https://doi.org/10.1007/s00382-015-2581-6)
- Berbery EH, Nogueira-Paegle J, Horel JD (1992) Wavelike southern hemisphere extratropical teleconnections. *J Atmos Sci* 49:155–177
- Carvalho LMV, Jones C, Liebmann B (2004) The South Atlantic convergence zone: intensity, form, persistence, relationships with intraseasonal to interannual activity and extreme rainfall. *J Clim* 17:88–108
- Chen M, Shi W, Xie P, Silva VBS, Kousky VE, Higgins RW, Janowiak JE (2008) Assessing objective techniques for gauge-based analyses of global daily precipitation. *J Geophys Res* 113:D04110. doi:[10.1029/2007JD009132](https://doi.org/10.1029/2007JD009132)
- Cunningham CC, Cavalcanti IFA (2006) Intraseasonal modes of variability affecting the South Atlantic convergence zone. *Int J Climatol* 26:1165–1180
- Gan AM, Rao VB (1994) The influence of the Andes Cordillera on transient disturbances. *Mon Weather Rev* 122:1141–1157
- Garreaud RD (2000) Cold air incursions over subtropical South America: mean structure and dynamics. *Mon Weather Rev* 128:2544–2559
- Grimm AM, Silva Dias PL (1995) Analysis of tropical-extratropical interaction with influence functions of a barotropic model. *J Atmos Sci* 52:3538–3555
- Hirata F, Grimm AM (2015) The role of synoptic and intraseasonal anomalies on the life cycle of summer rainfall extremes over southeastern South America. *Clim Dyn*. doi:[10.1007/s00382-015-2751-6](https://doi.org/10.1007/s00382-015-2751-6)
- Hoskins BJ, Ambrizzi T (1993) Rossby wave propagation on a realistic longitudinally varying flow. *J Atmos Sci* 50:1661–1671
- Jones C, Waliser DE, Lau KM, Stern W (2004) Global occurrences of extreme precipitation and the Madden-Julian Oscillation: observations and predictability. *J Clim* 17:4575–4589
- Kalnay E, Kanamitsu M, Kistler R, Collins W, Deaven D, Gandin L, Iredell M, Saha S, Woollen J, Zhu Y, Chelliah M, Ebisuzaki W, Higgins W, Janowiak J, Mo KC, Ropelewski C, Wang J, Leetma A, Reynolds R, Jenne R, Joseph D (1996) The NCEP-NCAR 40 year reanalysis project. *Bull Am Meteorol Soc* 77:437–471
- Liebmann B, Smith CA (1996) Description of a complete (interpolated) outgoing longwave radiation dataset. *Bull Am Meteorol Soc* 77:1275–1277
- Liebmann B, Kiladis GN, Marengo JA, Ambrizzi T, Glick JD (1999) Submonthly convective variability over South America and the South Atlantic convergence zone. *J Clim* 12:1877–1891
- Liebmann B, Kiladis GN, Vera CS, Saulo AC, Carvalho LMV (2004) Subseasonal variations of rainfall in South America in the vicinity of the low-level jet east of the Andes and comparison to those in the South Atlantic convergence zone. *J Clim* 17:3829–3842
- Livezey RE, Chen WY (1983) Statistical field significance and its determination by Monte Carlo techniques. *Mon Weather Rev* 111:46–59
- Marengo JA, Cornejo A, Satyamurty P, Nobre C, Sea W (1997) Cold surges in tropical and extratropical South America: the strong event in June 1994. *Mon Weather Rev* 125:2759–2786
- Mo KC, Higgins RW (1998) The Pacific–South American modes and tropical convection during the Southern Hemisphere winter. *Mon Weather Rev* 126:1581–1596
- Mo KC, Nogués-Paegle J (2001) The Pacific–South American modes and their downstream effects. *Int J Climatol* 21(10):1211–1229
- Nogués-Paegle J, Mo KC (1997) Alternating wet and dry conditions over South America during summer. *Mon Weather Rev* 125:279–291
- Nogués-Paegle J, Byerle LA, Mo KC (2000) Intraseasonal modulation of South American summer precipitation. *Mon Weather Rev* 128:837–850
- Tedeschi RG, Grimm AM, Cavalcanti IFA (2015) Influence of Central and East ENSO on extreme events of precipitation in South America during austral spring and summer. *Int J Climatol* 35:2045–2064. doi:[10.1002/joc.4106](https://doi.org/10.1002/joc.4106)
- Vera CS, Vigliarolo PK (2000) A diagnostic study of cold air outbreaks over South America. *Mon Weather Rev* 128:3–24
- Webster PJ, Chang H-R (1988) Energy accumulation and emanation at low latitudes: impacts of a zonally varying basic state. *J Atmos Sci* 45:803–829
- Wheeler MC, Hendon HH (2004) An all-season real-time multivariate MJO index: development of an index for monitoring and prediction. *Mon Weather Rev* 132:1917–1932